Acta Cryst. (1978). A**34**, 765–773

Electron-Microscope Study of the Crystal Structures of Mixed Oxides in the Systems Rb_2O–Ta_2O_5, Rb_2O–Nb_2O_5 and K_2O–Ta_2O_5 with Composition Ratios Near 1:3. I. Stacking Characteristics of MO_6 Layers

BY K. YAGI*

Physics Department, Arizona State University, Tempe, AZ 85281, *USA*

AND R. S. ROTH

National Bureau of Standards, Washington, DC 20234, *USA*

(*Received* 13 *January* 1978; *accepted* 15 *March* 1978)

The crystal structures of phases, previously designated as 11*L*, 9*L* and 16*L*, which were commonly found in the title systems are suggested from their high-resolution two-dimensional electron-microscope images. Two types of blocks are found which are composed of five and six layers of pentavalent-metal oxide octahedra and are closely related to the pyrochlore structure. The 11*L* structure is of rhombohedral ABCABC stacking of the former type of block, and the 9*L* structure is of hexagonal $B_0A'_0B_0A'_0$ stacking of the latter type of block. The 16*L* structure is found to be an alternate stacking of the two types of blocks. The method of stacking of the blocks is the same for the three structures and is found to be favorable from the point of view of local charge balance.

1. Introduction

Mixed crystals of alkali oxides and pentavalent transition metal oxides were extensively studied by one of the present authors (RSR) and his co-workers in order to find phases which might show interesting ionic conductivity. Phase-diagram studies and X-ray diffraction analyses were summarized in a recent review report [Roth, Brower, Parker, Minor & Waring (1975) with details given by Minor, Roth, Parker & Brower (1977)]. Among the many phases reported there, three distinct phases were found to exist commonly in the mixed oxides of Rb_2O–Ta_2O_5, Rb_2O–Nb_2O_5 and K_2O–Ta_2O_5 with composition ratios near 1:3 (Fig. 1). They were called 9*L*, 11*L* and 16*L* structures simply because the lattice parameters along their hexagonal *c* axes are close to integer multiples of the thickness of an MO_6 octahedron layer (about 4 Å), where *M* is a pentavalent metal. The extinction rules and probable space groups were also mentioned in the report and are given in Table 1. However, the extinction rules are not compatible with the above-mentioned integer numbers.† Therefore, these integer numbers are used only for convenience and it will be shown in part II (Yagi & Roth, 1978) that another notation is more suitable to describe these phases and other various intergrowth phases.†

While specimens of these single crystals prepared at the National Bureau of Standards were investigated with X-rays by Gatehouse and his co-workers at Monash University in Melbourne, Australia, powder samples were also investigated by high-resolution electron microscopy at Arizona State University. Although the high-resolution two-dimensional structure-imaging method with a resolution of about 3·5 Å, developed by Iijima (1971) and Cowley & Iijima (1973), does not give individual atom positions, it does give some structural information such as the arrangements of metal–oxygen octahedra in transition-metal oxides. This series of papers describes the results obtained by an electron-microscope study.

In part I, the arrangements of octahedra in the 11*L*, 9*L* and 16*L* structures proposed from electron-microscope images are described. In part II, the following paper, the structures of various intergrowth phases and two-dimensional ordering of pentavalent ions will be

* Present address: Physics Department, Tokyo Institute of Technology, Oh-okayama, Meguro-ku, Tokyo 152, Japan.

† For example, if the 11*L* structure is composed of 11 layers of octahedra, it is difficult to deduce the observed possible reflection condition, $-h + k + l = 3n$ (Table 1), from the 11 layers, because 11 is not an integer multiple of 3.

† In this notation the structures are expressed by the numbers of two types of block in the unit cells, which are composed of five and six layers of pentavalent-metal oxide octahedra. The 11*L*, 9*L* and 16*L* structures are expressed by 1-0 *R*, 0-1 *H* and 1-1 *H*, respectively (see part II) and they are written in all the micrographs and the diffraction patterns.

Table 1. *X-ray data for the* Rb_2O–Nb_2O_5 *system*

Designation	mol %	Symmetry	a (Å)	c (Å)	Possible reflections	Probable space group
11 L	26·67	Hexagonal	7·522	43·18	hkl: $-h+k+l=3n$	$R3$, $R\bar{3}$, $R32$, $R3m$, $R\bar{3}m$
16 L	25·5	Hexagonal	7·514	65·12	hhl: $l=2n$	$P6_3mc$, $P\bar{6}2c$, $P6_3mmc$
9 L	25	Hexagonal	7·518	36·353	hhl: $l=2n$	$P6_3mc$, $P\bar{6}2c$, $P6_3mmc$

given, and the obtained images will be compared with the computed images, which are based on the proposed octahedron and ion arrangements.

2. Experimental techniques

The preparation of the sample crystals was described elsewhere (Roth, Brower, Parker, Minor & Waring, 1975). The specimens listed in Table 2 were used for the present study. A JEM 100B electron microscope modified for high-resolution work was used (Iijima, 1971). Sample crystals were ground in an agate mortar and fine fragments were collected on holey carbon films. Very thin crystallites were selected and tilted inside the microscope so that the electron beam was parallel to the crystallographic axes, either $[010]_h$ or $[001]_h$.*

3. Results

3.1 *The* 11L *structure*

Fig. 2 shows a diffraction pattern and the corresponding electron micrograph with aperture size shown in (*a*) from an 11L crystallite of sample No. 4. The

*In this paper, the hexagonal system was used to express the crystallographic axes and planes for the 11L, 9L and 16L structures.

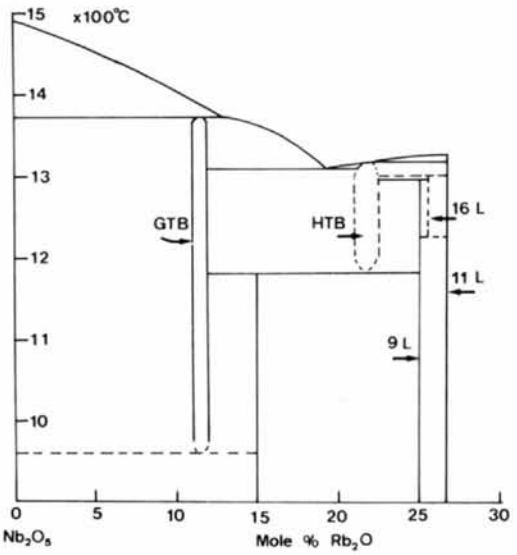

Fig. 1. Phase diagram for Nb_2O_5–Rb_2O after Roth, Brower, Parker, Minor & Waring (1975).

Table 2. *List of sample crystals*

Specimen No.	System	mol %	X-ray data
1	Rb_2O–Nb_2O_5	25·5	9 L
2		26·67	11 L
3	Rb_2O–Ta_2O_5	25	9 L
4		26·67	11 L
5	K_2O–Ta_2O_5	26·33	9 L + 16 L
6		26·5	16 L
7		28·57	11 L

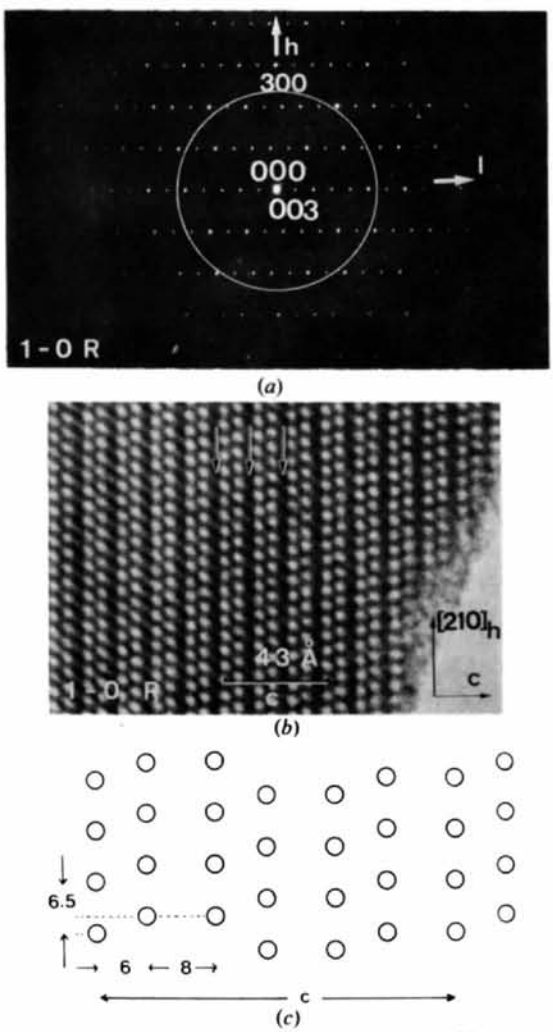

Fig. 2. (*a*) An electron diffraction pattern and (*b*) the corresponding electron micrograph of an 11L crystallite for $[010]_h$ incidence. The arrangement of white spots in (*b*) is schematically shown in (*c*). The objective-aperture size is shown in (*a*).

incident beam is parallel to the $[010]_h$ axis. The diffraction pattern is indexed, for convenience, using the hexagonal unit cell given in Table 1. It is seen that the extinction rule (reflection forbidden for $-h + k + l = 3n \pm 1$) in Table 1 is satisfactorily reproduced in the pattern. The electron micrograph (*b*), and all the micrographs shown in this series of papers, were taken with defocus values around −900 Å, which is the optimum defocus for the structure image with the present apparatus. In (*b*) regular arrays of white dots, which are schematically reproduced by circles in (*c*) are seen. White dots along the $[210]_h$ direction, perpendicular to the *c* axis, are spaced by 6·5 Å, which corresponds to the $(100)_h$ lattice spacing. Two successive white-spot arrays separated by about 6 Å are seen to make units which join each other at the dark lines indicated by arrows. Within each unit, the white spots have a relative shift of about one third of 6·5 Å parallel to the $[210]_h$ direction. It should be noted that there is no shift between the positions of neighboring white spots spaced 8 Å apart across the dark lines. Therefore, six white-spot arrays, *i.e.* three units of the same structure, form a unit-cell distance (~43 Å) along the *c* axis.

If the notation *abc* is used to describe the positions of white spots along $[210]_h$ as used for the atom positions of {111} planes in f.c.c. metals, a sequence of white-spot positions along the *c* axis can be written as *-ab-bc-ca-* where hyphens denote the positions of dark lines.

Fig. 3 shows an electron diffraction pattern of $[001]_h$ incidence and the corresponding electron micrograph of an 11*L* crystallite from sample No. 4. In (*a*), $\{hk0\}$ reflections with $-h + k = 3n \pm 1$ are absent in agreement with the extinction rule in Table 1. In the electron micrograph no strong lattice image corresponding to $\{100\}_h$ type reflections of 6·5 Å spacing is seen, as a natural consequence of the absence of the $\{100\}_h$ type reflection. However, in the area near the crystal edge, indicated by arrows, where the crystallite is very thin, hexagonal arrangements of white spots or black spots of spacing corresponding to $\{100\}_h$ type reflections are seen.

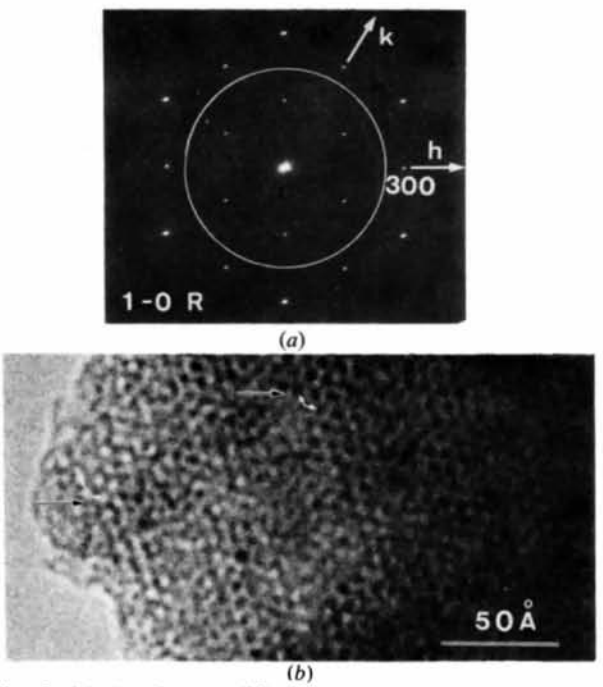

(*a*)

(*b*)

Fig. 3. (*a*) An electron diffraction pattern and (*b*) the corresponding micrograph of an 11*L* crystallite for $[001]_h$ incidence. The arrows in (*a*) show the reciprocal directions of $[h00]_h$ and $[0k0]_h$.

3.2. *The 9L structure*

Figs. 4–6 show observations for the 9*L* structure. In an electron diffraction pattern of $[100]_h$ incidence in Fig. 4(*a*), the $\{00l\}$ reflections with l = odd are seen. However, their appearance is due to double diffraction.

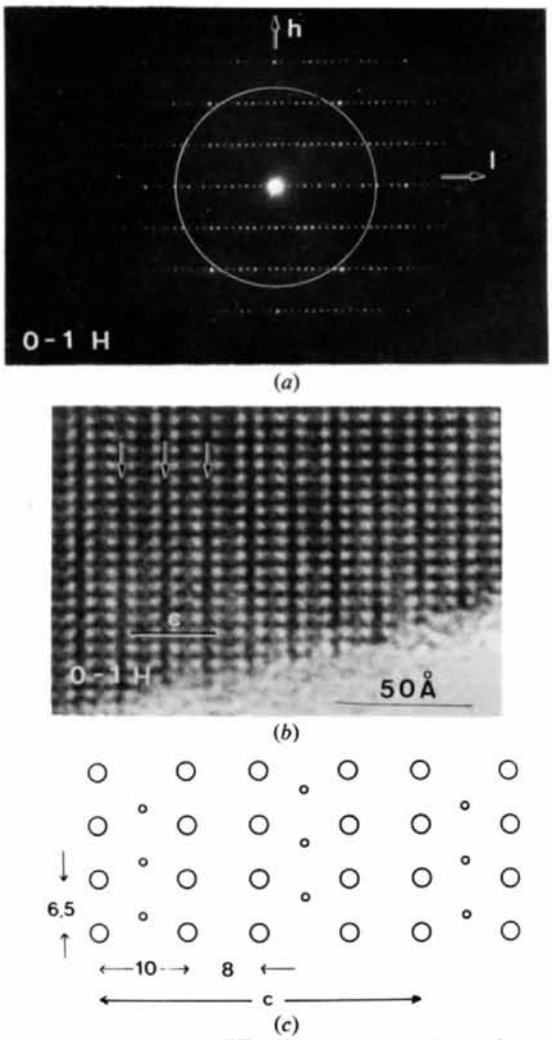

(*a*)

(*b*)

(*c*)

Fig. 4. (*a*) An electron diffraction pattern and (*b*) the corresponding electron micrograph of a 9*L* crystallite for $[010]_h$ incidence. The arrangement of the white spots in (*b*) is schematically shown in (*c*).

In the case of $[\bar{1}10]_h$ incidence, the $(00l)$ reflections as well as the (hhl) reflections with l = odd are absent. Again, the extinction rule for the $9L$ structure in Table 1 is reproduced.

The electron micrograph in Fig. 4(*b*) shows vertical white-spot arrays with a spot spacing of about 6·5 Å, as schematically shown in (*c*). Two arrays spaced about 10 Å apart form a unit in the micrograph, and between them are less-distinct white regions. The positions of white spots in the unit do not shift relative to each other. The units are seen to adjoin at the dark lines indicated by arrows, across which the positions of the white spots do not shift as in the case of the $11L$ structure.

The image contrast of the white regions at the center of the unit is very sensitive to the crystal orientation and amount of defocus. However, it was found that the positions of the central spots in the neighboring units are not the same, as schematically shown in Fig. 4(*c*). A micrograph which shows the difference very clearly in an exaggerated way is shown in Fig. 5. The crystallite in this case is not in an exact $[110]_h$ orientation.

Fig. 6 shows the electron diffraction pattern of $[001]_h$ incidence and the corresponding micrograph from a $9L$ crystallite. All $(hk0)$ reflections are seen in (*a*). In (*b*), a hexagonal arrangement of black spots due to the $\{100\}_h$ reflections is seen in the region where the crystal is relatively thin.

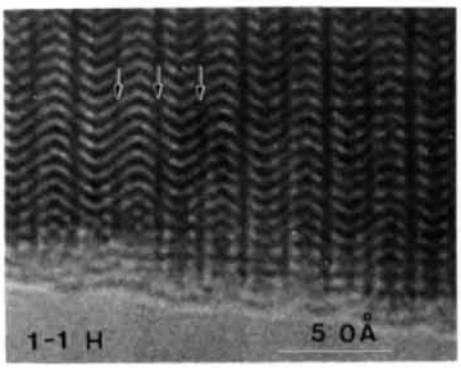

Fig. 5. An electron micrograph of a $9L$ crystallite. The incident beam is not exactly parallel to the $[010]_h$ direction. The difference in structure between the neighboring units, which is not clear in Fig. 4(*a*) and is shown by the different positions of small circles in Fig. 4(*c*), is seen in an exaggerated way. The arrows indicate the positions of dark lines.

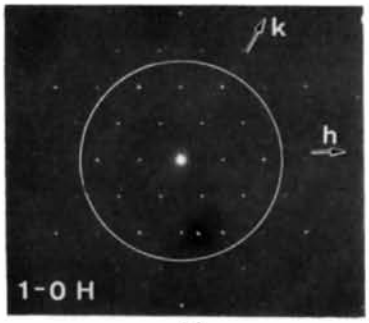

(*a*)

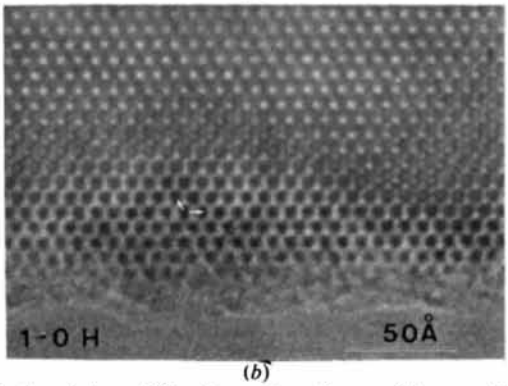

(*b*)

Fig. 6. An electron diffraction pattern from a $9L$ crystallite for $[001]_h$ incidence. The arrows indicate the $[h00]_h$ and $[0k0]_h$ reciprocal directions. A corresponding image in (*b*) shows the hexagonal arrangement of black spots in thin regions.

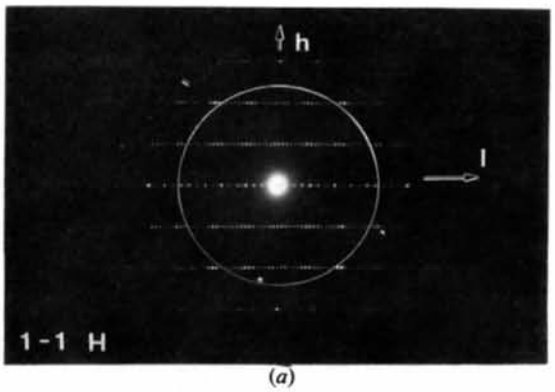

(*a*)

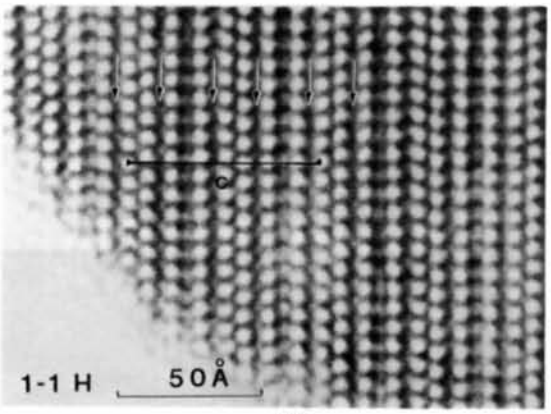

(*b*)

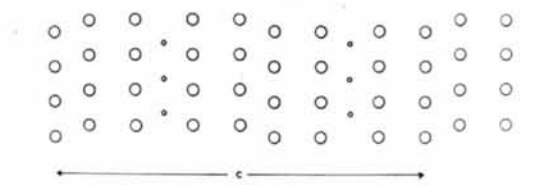

(*c*)

Fig. 7. A $16L$ crystallite for $[010]_h$ incidence.

3.3. *The 16L structure*

Fig. 7 shows an electron diffraction pattern and the corresponding electron micrograph of a K_2O–Ta_2O_5 crystallite (sample No. 6 in Table 2) for the $[010]_h$ orientation. In (*a*), the appearance of $(00l)_h$ reflections with l = odd is due to multiple diffraction as in the case of the 9*L* structure in Fig. 4. The extinction rules given in Table 1 are again consistent with the present observation. In the micrograph (*b*), vertical white-spot arrays are seen with spot spacing about 6·5 Å and dark bands indicated by arrows, which are commonly observed in the cases of the 11*L* and 9*L* structures. The arrangement of the white spots is schematically shown in (*c*). By comparing it with Figs. 2(*c*) and 4(*c*), it is easily concluded that the 16*L* structure is made up of alternate stacking of two kinds of blocks found in the 11*L* and 9*L* structures.

Fig. 8 shows an electron diffraction pattern and the corresponding micrograph of a 16*L* crystallite for $[001]_h$ incidence. In (*b*), a hexagonal arrangement of white spots is seen, but at very thin regions a hexagonal arrangement of black spots is seen as indicated by the white arrow. Note that in (*a*) very weak reflections are seen at the center of the hexagonal $(hk0)_h$ reflections as indicated by arrows. This fact suggests the existence of a $\sqrt{3}a$ superstructure lattice, where a is the unit-cell parameter of the hexagonal lattice. Since these reflections are very weak, the image in (*b*) does not show such a superlattice.

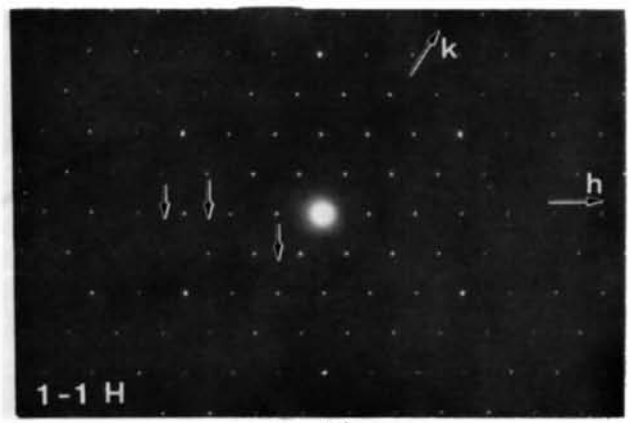

(*a*)

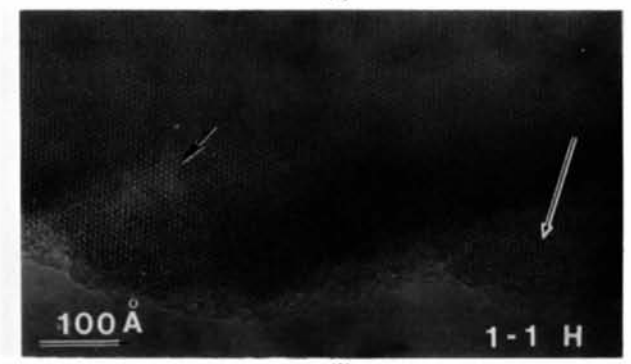

(*b*)

Fig. 8. A 16*L* crystallite for $[001]_h$ incidence. Faint spots, which can be clearly seen on the original photograph and which are at the positions indicated by vertical arrows in (*a*), show a $\sqrt{3}a$ superstructure lattice.

4. Proposed structural model

From the fact that the a parameters of 11*L*, 9*L* and 16*L* are about 7·5 Å, their structures were suggested in the previous review paper (Roth, Brower, Parker, Minor & Waring, 1975) to be made up of ordered sequences of the two kinds of layers of octahedra in the pyrochlore structure. Before describing the models for them, it is worth while to describe the structure characteristics of the pyrochlore structure.

4.1. *The pyrochlore structure*

Fig. 9 shows the arrangement of octahedra in the pyrochlore structure. In (*a*), the MO_6 octahedron arrangement in the (111) layer is shown. It is identical with that of the basal plane of the hexagonal tungsten bronze (HTB) structures except that octahedra are tilted so as to form small triangles of the top oxygen atoms at the positions designated by *A* and large triangles at *C*. The bottom oxygen atoms, on the other hand, form large triangles at *A* and small ones at *C*. The large hexagonal holes are at positions *B*. In the pyrochlore structure, an isolated octahedron layer corner-shares with the HTB-like layer so that one of the triangles of the overlying octahedron coincides with the small triangle of the top oxygen layer. On this isolated octahedron layer, another HTB-like layer corner-shares so as to fit its small bottom-oxygen triangles with another set of triangles of isolated octahedra as shown in (*b*). The position of the hexagonal hole in this second HTB-like layer is at *C* in Fig. 9(*a*). We denote the first layer by *A*, the second isolated octahedron layer by *a* and the third layer by *B*. Then, the pyrochlore structure can be written as *AaBbCcA* ..., as shown in Table 3(*a*). The side view of the structure from the $[010]_h$ direction indicated in Fig. 9(*b*) is shown in Fig. 9(*c*). The darker octahedra indicate where the octahedron density along the projection direction is twice as large as for other positions. Note that at the isolated octahedron layer there exists a hole array. The hole distance is about 6·5 Å and the spacing between the neighboring arrays is about 6·1 Å. The positions of the holes shift by 6·5/3 Å between the neighboring arrays. The simple phase-grating approximation for electron-microscope image formation indicates that white spots should be seen at the positions of these holes in high-resolution micrographs of the pyrochlore structure if they are seen from the $[010]_h$ direction under an optimum defocus condition and there are no heavy atoms along the holes.

Hence the white-spot positions, *i.e.* the hole sequence along the $[001]_h$ direction, can be written as *abcabc* . . . as shown in Table 3(*a*). We can also construct the pyrochlore structure starting from the HTB-like layer of Fig. 9(*a*), but its octahedra are tilted in an opposite sense. In this case small oxygen triangles are formed at *C* positions so that the structure may be written as *A'c'C'b'B'a'A'* . . . and the hole-position sequence may be expressed as *cbacba* . . ., where *A'* means the mirror structure of *A* and so on, as indicated in Table 3(*a*).

4.2. *Proposed model for the* 11*L structure*

From these considerations, it is quite natural to conclude that the arrays of two white spots forming a unit in Fig. 2 are portions of the pyrochlore structure, such as *AaBbC*. Then, the problem to solve is how such units are stacked to form the dark lines in Fig. 2. The stacking model should be compatible with the three observed facts: (1) The metal-atom density, *i.e.* octahedron density, is high at the dark line. (2) The positions of the white spots across the dark line are the same. (3) The spacing of two white-spot arrays across the dark line is about 8 Å. The proposed model for the stacking at the dark lines for the 11*L* structure is shown in Fig. 10 and Table 3(*b*). A high-density octahedron region is formed. It should be noted that the hole positions do not change across the double layer of the HTB-like layer and that the distance of holes across it is about 8 Å (6 + 2). Since the lattice fitting between the two layers is not good if the layers are rigid HTB-like ones, as in the pyrochlore structure, some sort of rearrangement of oxygen atoms is necessary.* However,

* A similar stacking sequence of metal oxygen octahedra was reported independently by Gatehouse (1976) and by Groult, Chailleux, Choisnet & Raveau (1976) in the cases of $K_6Ta_{15\cdot6}O_{42}$ and $K_3Nb_8O_{21}$ respectively. The presence of the above-mentioned stacking in the 11*L* structure was privately communicated to one of the present authors (RSR) by Dr B. M. Gatehouse, although the overall refined structure was not available during interpretation of the micrographs.

Table 3. *Stacking sequences in the four structures*

	Structures	Stacking sequence of octahedron layers	Hole-position sequence
(*a*)	Pyrochlore structure	*AaBbCcAa*...	*abcabc*...
	(mirror structure)	*A'c'C'b'B'a'A'c'*...	*cbacba*...
(*b*)	11 *L* Structure (1-0 *R*)	*AaBbCBbCcACcAaBAaBbC*... (B C A B)	*ab-bc-ca-ab*...
	(mirror structure)	*A'c'C'b'B'C'b'B'a'A'B'a'A'c'C'A'c'C'b'B'*... (C' B' A' C')	*cb-ba-ac-cb*...
(*c*)	9 *L* Structure (0-1 *H*)	*AaBB'a'A'B'a'A'AaBAaBB'a'A'*... (B_0 A'_0 B_0)	*aa-aa-aa*...
(*d*)	16 *L* Structure (1-1 *H*)	*AaBbCBbCC'b'B'C'b'B'a'A'B'a'A'AaB*... (B C_0 B' A'_{0*})	*ab-bb-ba-aa-ab*...

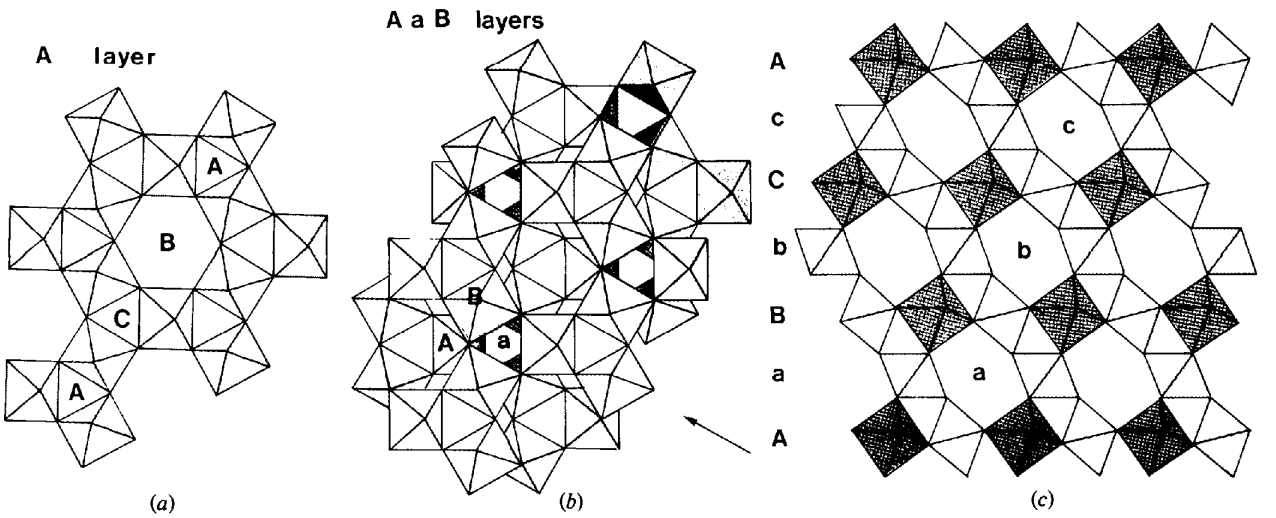

Fig. 9. Characteristic arrangement of octahedra in the pyrochlore structure. (*a*) HTB-like layer in the pyrochlore structure. (*b*) *AaB* layer stacking in the pyrochlore structure. (*c*) Side view of the pyrochlore structure seen from the direction shown in (*b*).

it is expected that the rearrangement is not such as to form ideal HTB layers because the rules of stacking beyond the double layer are those expected in the pyrochlore structure; this point will be discussed in part II.

The sequence of stacking in the $11L$ structure is, therefore, *AaBbCBbCcACcAaBAa* ... and the hole-position sequence is *ab-bc-ca-ab-*, where hyphens indicate the positions of double layers. For convenience we call the *AaBbC* layer a five-layer block and denote it by B since the central layer is *B*. So that the $11L$ structure can be expressed as a rhombohedral stacking of the five-layer blocks: BCABCA, where the five-layer blocks are connected to each other to form the double layers mentioned above. A structure with a mirror relation to BCA is also possible, as shown in Table 3(*b*).

The positions of the alkali-metal ions are difficult to estimate from the images. The ions are expected to be positioned in the isolated octahedron layers and in the hexagonal holes in the HTB-like layers. The arrangement should satisfy the extinction rule in Table 1.

In the present $11L$ model, all kinds of pyrochlore layers, *ABCabc*, are equally present in the unit cell, so the positions *A*, *B* and *C* in Fig. 9(*a*) are equivalent. This is the reason why the $\{100\}_h$ and $\{200\}_h$ type reflections are absent, and the distinct $\{100\}_h$ lattice images are not seen in Fig. 3(*b*). However, the thickness of the crystallite is not always an integer multiple of the unit-cell length ($c \sim 43$ Å). In such areas the three positions are not equivalent and we can expect a hexagonal arrangement of white or black spots in the micrographs. For example, when the thickness corresponds to *n* unit cells plus *AaB* layers (Fig. 9*b*) the positions *A* are expected to be dark and in the case of excess *AaBbC* layers, position *C* should be bright in the images. The relative deviations from the average of the three positions are large for small *n* values. This may be the reason for the appearance of the hexagonal arrangement of black and white spots in thin regions in Fig. 3(*b*).

4.3. *Proposed model for the 9L structure*

A similarity in the white-spot arrangement across the dark lines in Figs. 2(*b*) and 4(*b*) indicates that the double HTB-like layers shown in Fig. 10 are also present in the $9L$ structure. The problem is to propose a structural model for the block between the successive dark lines. The model should be compatible with three facts: (1) Two white-spot positions in the block are the same. (2) The separation between them is about 10 Å. (3) There are relatively low metal-atom density regions at the center of the block. The proposed model for the block is composed of six octahedron layers as is shown in Fig. 11. The center of the block is a mirror plane and there is a small-hole array. The stacking sequence of the $9L$ structure is *AaBB'a'A'B'a'A'AaBA* ... and is shown in Table 3(*c*). The hole-position sequence is *aa-aa* ..., where the hyphen indicates the position of a double layer. Although the images of neighboring blocks are seen to be similar in Fig. 4(*b*), the central two successive HTB-like layers are different, *i.e. BB'* and *A'A* and this difference is more clearly seen in Fig. 5. It is convenient to denote the six-layer block *AaBB'aA'* by B_0, since central layers are *BB'*, then the $9L$ structure can be expressed as $B_0A'_0B_0A'_0$: a hexagonal stacking of the six-layer blocks.

From the stacking sequence in Table 3(*c*), it is seen that *C'* and *C* layers are absent and only *a* and *a'* type isolated octahedron layers exist. These two factors increase the $[001]_h$ projected potential at the *A* positions in Fig. 9(*a*) in comparison with the case where

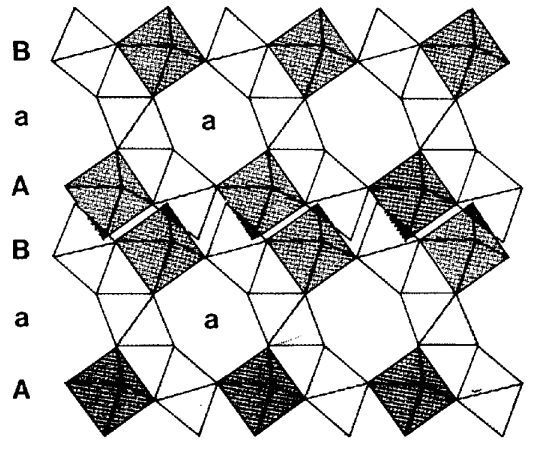

Fig. 10. The structural model for the dark band in Fig. 2(*b*). The rearrangement of the oxygen atoms is necessary to achieve a good fit to form a double HTB-like layer sequence. Note that the hole position is the same, *a*, across the double layer.

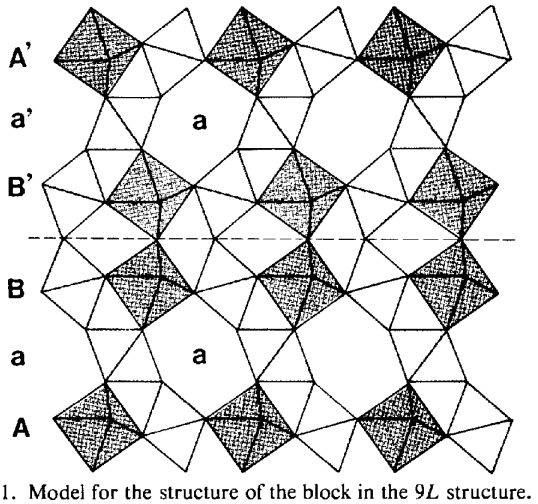

Fig. 11. Model for the structure of the block in the $9L$ structure. A mirror plane is formed between two successive HTB-like layers *BB'*. Note that the hole position is the same, *a*, across the successive HTB-like layers.

A, *B*, *C* and *a*, *b*, *c* layers are equally present. Therefore, the images with $[001]_h$ incidence are expected to show a hexagonal arrangement of black spots in agreement with the observation in Fig. 6(*b*). The above mentioned argument still holds even if the thickness of the crystal is a fraction of the unit-cell length.

As in the case of the 11*L* structure, the positions of the alkali-metal ions are uncertain.

4.4. *Proposed model for the* 16*L structure*

From Fig. 7(*b*), it is very easy to propose a structural model for the 16*L* structure: alternate stacking of the five and six-layer blocks, which are shown in Table 3(*d*). The stacking sequence of the octahedron layers is *AaBbCBbCC'b'B'C'b'B'a'A'AaBAa*..., and the hole-position sequence is *ab-bb-ba-aa-ab*.... By using the notations for the five and six-layer blocks, the 16*L* can be written as $BC_0B'A'_0$....

Since in this model the *c* and *c'* layers are absent and there are more *B* layers than *A* and *C* layers, the positions of the octahedra in the *c* layer, position *C* in Fig. 9(*a*), should be seen as a white spot in the image of $(001)_h$ incidence. If the specimen is so thin as to be composed of, for example, only BC_0 in Table 3(*d*), the positions of the octahedra in the *b* layer should be seen as black spots. These are in agreement with the observed image features in Fig. 8(*b*).

5. Discussion

The structure models for the 11*L*, 9*L* and 16*L* were proposed from the high-resolution structure images. They are found to be composed of two types of blocks of five and six octahedron layers and they are stacked in the same way so as to form double HTB-like layers. The lattice fit between the blocks is not good if we consider the rigid HTB-like layers, so a rearrangement must take place which should be shown by the refined X-ray structure study (Fallon & Gatehouse, 1977). However, it should be noted here that the rearrangements are not such that the HTB-like layers become the exact HTB layer. If the latter occurred, the *CB* and *BC* stacking and the *CBa* and *CBb* stacking should have been found, contrary to the observations. This fact suggests that octahedra in the double layer are still tilted so as to fit well with the neighboring isolated-octahedron layer to form sequences such as *Bb*.

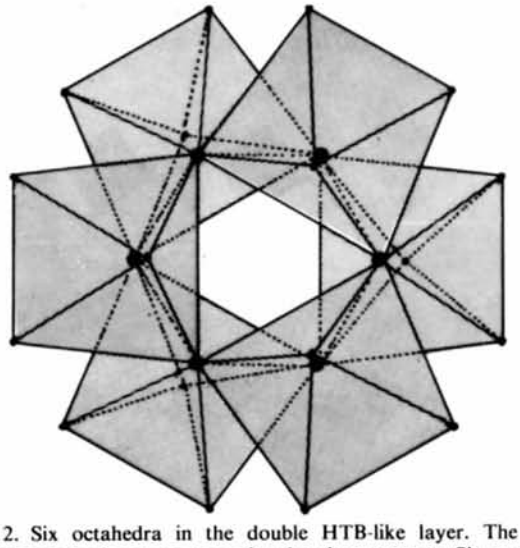

Fig. 12. Six octahedra in the double HTB-like layer. The rearrangement of oxygen atoms is taken into account. Six oxygen ions are completely shared by the six pentavalent metal ions at the centers of the octahedra and 18 oxygen ions are at octahedron corners shared by one of the six ions and ions in other layers. Therefore, charge balance is locally satisfied.

It is this kind of tilting which produces the sequence rules of the two kinds of blocks found in the present study. Using the notation in Table 3, the rules are as follows: AB_0, AB_0 (and cyclic combinations), $A'C'$, $A'C'_0$ (and cyclic combinations), A_0C', $A_0C'_0$ (and cyclic combinations), A'_0B, A'_0B_0 (and cyclic combinations). It will be shown in part II that these rules play an important role in determining the structure and symmetry of the various intergrowth phases.

Although octahedra must be distorted to make a good fit at the double HTB-like layer, this double layer is favorable from consideration of local charge balance. In this configuration six pentavalent transition atoms share 15 oxygen atoms as shown in Fig. 12, and therefore the charge balance is locally satisfied. The alkali-metal ions are, therefore, expected to be accommodated in the isolated-octahedron layer and the hexagonal holes of the HTB-like layers which do not form double layers. The alkali ions compensate the excess negative charges in *aBb* for the five-layer block and *aBB'a'* for the six-layer block. However, if this were the only consideration, the 11*L* structure should have been on the left side of the 9*L* structure in the phase diagram in Fig. 1. To explain the observed order, it is necessary to introduce Nb atoms at the mirror plane in the six-layer block to obtain the local charge balance. It will be shown in part II that in the 16*L* structure of the K_2O–Ta_2O_5 system two-dimensional ordering of Ta atoms was actually observed at the mirror plane between the two successive HTB-like layers to form the $\sqrt{3}a$ structure. The very weak superstructure spot in Fig. 8(*a*) is due to this kind of ordering. Although the details will be given in part II, it should be mentioned that the presence of transition metals at the mirror plane may be one reason why the images at the center of the six-layer block do not show clear white spots. The fact that the hole size there is close to the limit of resolution may be another reason. It is important to compare the observed images with the calculated images based upon the proposed models. This will be given in part II.

One of the present authors (KY) expresses his sincere thanks to Professor J. M. Cowley for providing him with the opportunity to stay at ASU and for his continuous encouragement. Thanks are also due to Dr S. Iijima for much technical advice and discussion concerning high-resolution electron microscopy. This work was partially supported by the Ministry of Education of Japan and by USA National Science Foundation grants GH 36668 and DMR 76-06108.

References

COWLEY, J. M. & IIJIMA, S. (1973). *Z. Naturforsch. Teil A*, **27**, 445–451.

FALLON, G. D. & GATEHOUSE, B. M. (1977). *J. Solid State Chem.* **22**, 405–409.

GATEHOUSE, B. M. (1976). *J. Less-Common Met.* **50**, 139–144.

GROULT, D., CHAILLEUX, J. M., CHOISNET, J. & RAVEAU, B. (1976). *J. Solid State Chem.* **19**, 235–244.

IIJIMA, S. (1971). *J. Appl. Phys.* **42**, 5891–5893.

MINOR, D. B., ROTH, R. S., PARKER, H. S. & BROWER, W. S. (1977). *J. Res. Natl Bur. Stand.* **82**, 151–165.

ROTH, R. S., BROWER, W. S., PARKER, H. S., MINOR, D. B. & WARING, J. L. (1975). *NASA Contract. Rep.* CR-134869.

YAGI, K. & ROTH, R. S. (1978). *Acta Cryst.* A**34**, 773–781.

Acta Cryst. (1978). A**34**, 773–781

Electron-Microscope Study of Crystal Structures of Mixed Oxides in the Systems Rb_2O–Ta_2O_5, Rb_2O–Nb_2O_5 and K_2O–Ta_2O_5 with Composition Ratios Near 1:3. II. Various Intergrowth Phases and Two-Dimensional Ordering of Pentavalent Ions

BY K. YAGI*

Physics Department, Arizona State University, Tempe, AZ 85281, *USA*

AND R. S. ROTH

National Bureau of Standards, Washington, DC 20234, *USA*

(*Received* 13 *January* 1978; *accepted* 15 *March* 1978)

In part I, the preceding paper, structural models were proposed on the basis of high-resolution electron microscopy for phases previously designated as 11*L*, 9*L* and 16*L*, which were found to exist in the title systems. Two types of blocks were found, which are composed of five and six layers of octahedra. In the present paper, various intergrowth phases which are composed of the two types of blocks are described. A new notation is proposed to denote these intergrowth phases as well as the 11*L*, 9*L* and 16*L* structures. Two-dimensional ordering of pentavalent ions in the six-layer block is found, giving rise to diffuse scattering in electron diffraction patterns. Two-dimensional images, calculated on the basis of the proposed model, are found to reproduce the observed images.

1. Introduction

In part I (Yagi & Roth, 1978) structure models were proposed from the high-resolution structure images taken in a modified high-resolution microscope (Iijima, 1971) for the 11*L*, 9*L* and 16*L* structures which were found to exist commonly in the mixed oxides Rb_2O–Nb_2O_5, Rb_2O–Ta_2O_5 and K_2O–Ta_2O_5. The structures are closely related to the pyrochlore structure and are summarized in Table 1. In the pyrochlore structure, hexagonal tungsten bronze (HTB) like octahedron layers and isolated-octahedron layers are alternately stacked in the way *AaBbCc*.... Two types of blocks, which are composed of five and six octahedron layers,

Table 1. *Summary of structures*

Structures	Stacking sequences
Pyrochlore structure (mirror structure)	*AaBbCcAa*... *A'c'C'b'B'a'A'c'*...
11*L* structure (1-0 *R*) (mirror structure)	ABCABC... A'C'B'A'C'B'...
9*L* structure (0-1 *H*)	$B_0A'_0B_0A'_0$...
16*L* structure (1-1 *H*)	$BC_0B'A'_0BC_0B'$...
Sequence rules of blocks	AB, AB_0 (cyclic) A'C', $A'C'_0$ (cyclic) A_0C', $A_0C'_0$ (cyclic) A'_0B, A'_0B_0 (cyclic)
A : *CcAaB* (cyclic) A_0: *CcAA'c'C'* (cyclic)	A': *B'a'A'c'C'* (cyclic) A'_0: *B'a'A'AaB* (cyclic)

* Present address: Physics Department, Tokyo Institute of Technology, Oh-okayama, Meguro-ku, Tokyo 152, Japan.